RSC Advances

PAPER

View Article Online
View Journal | View Issue



Cite this: *RSC Adv.*, 2017, **7**, 11491

# Multifunctional $NaYF_4:Yb^{3+},Er^{3+}@SiO_2@Au$ heterogeneous nanocomposites for upconversion luminescence, temperature sensing and photothermal conversion

Dongdong Li,[a] Wen-Yong Lai,*[ab] Qiyue Shao*[c] and Wei Huang[ab]

Received 7th February 2017
Accepted 9th February 2017

DOI: 10.1039/c7ra01564j

rsc.li/rsc-advances

$NaYF_4:Yb^{3+},Er^{3+}@SiO_2@Au$ heterogeneous nanostructures, with the ability of integrating upconversion luminescence (UCL) and photothermal therapy as well as real-time temperature monitoring, have been successfully prepared. The UCL intensities of $NaYF_4:Yb^{3+},Er^{3+}$ nanocrystals showed an obvious reduction after gold nanoparticle attachment and gold shell coating, but it was found that they were independent of the $SiO_2$ spacer layer thicknesses. The presence of gold nanostructures can significantly improve the photothermal conversion properties of $NaYF_4:Yb^{3+},Er^{3+}$ nanocrystals with an increased temperature up to 39 °C, while retaining their temperature sensing properties, manifesting their great potential as diagnostic and therapeutic tools for use in biomedical fields.

## Introduction

Multifunctional nanostructures that are capable of combining various intrinsic properties in a single construct have received considerable attention due to their potential applications in multimodality imaging, biosensing, disease diagnosis, and therapy.[1–3] Lanthanide-doped upconversion nanoparticles (UCNPs), which are able to emit high-energy photons under excitation by near-infrared (NIR) light, have emerged as attractive materials to achieve these applications *in vitro* and *in vivo*.[4–8] Compared with the traditionally used down conversion fluorescent organic dyes and quantum dots, the use of NIR light as the excitation source provides UCNPs with many unique advantages such as low photobleaching, minimized autofluorescence and photodamage, and high penetration depth in biospecies, making them suitable for use as imaging, sensing and theranostic tools in biomedical fields.[9–11]

Among various UCNPs, hexagonal phase (β-)$NaYF_4:Yb^{3+},Er^{3+}$ nanoparticles have been demonstrated to be the most efficient upconversion materials.[12] However, their absolute quantum yields remain still low and are usually less than 1%.[13] Most of absorption energy has dissipated to crystal lattice as heat. Based on this reason, β-$NaYF_4:Yb^{3+},Er^{3+}$ UCNPs are potential novel photothermal therapy tools for clinical applications. Nevertheless, most previous efforts have been made to improve the UCL efficiency, but little has been attempted to utilize the heat energy generated from the photothermal conversion process. The use of $NaGdF_4:Yb^{3+},Er^{3+}$ nanocrystals alone is able to offer some heat energy, but the finite temperature increase (≤10 °C) in most cases was insufficient for photothermal therapy application.[14] The introduction of noble metal nanoparticles, especially gold and silver nanomaterials, is attractive to improve this performance, due to their strong optical absorption in visible and NIR range. Improved photothermal conversion properties have been achieved by constructing UCNPs@Au (or Ag) heterogeneous nanostructures.[15,16] However, their photothermal conversion efficiency is still unsatisfactory and only limited temperature rise no higher than 25 °C was recorded even at a high excitation power density.[16] Further optimization is highly desirable for realizing efficient photothermal conversion process.

In this work, $NaYF_4:Yb^{3+},Er^{3+}@SiO_2@Au$ heterogeneous nanostructures were designed, synthesized and efficient photothermal conversion was achieved by precisely controlling the particle size of Au nanoparticles and the thickness of Au shell. In order to clarify the controversial mechanism between noble metals and UCNPs, the influences of gold nanostructures (Au particles and Au shell) on the UCL properties were studied by accurately regulating $SiO_2$ isolation layer thicknesses. In addition, the temperature sensing application for the resulting heterogeneous nanostructures was also investigated. The results reveal that the presence of gold nanostructures can

[a]*Key Laboratory for Organic Electronics and Information Displays (KLOEID), Institute of Advanced Materials (IAM), Jiangsu National Synergetic Innovation Center for Advanced Materials (SICAM), Nanjing University of Posts & Telecommunications, 9 Wenyuan Road, Nanjing 210023, China. E-mail: iamwylai@njupt.edu.cn*

[b]*Key Laboratory of Flexible Electronics (KLOFE), Institute of Advanced Materials (IAM), Jiangsu National Synergetic Innovation Center for Advanced Materials (SICAM), Nanjing Tech University (NanjingTech), 30 South Puzhu Road, Nanjing 211816, China*

[c]*Jiangsu Key Laboratory of Advanced Metallic Materials, Department of Materials Science and Engineering, Southeast University, Nanjing 211189, People's Republic of China. E-mail: qiyueshao@seu.edu.cn*

significantly improve the photothermal conversion properties of $NaYF_4$:$Yb^{3+}$,$Er^{3+}$ nanocrystals with the increased temperature up to 39 °C, while retaining their temperature sensing properties.

## Experimental

### Sample preparation

The chemical reagents were all purchased from Sigma-Aldrich, and used without further purification. $NaYF_4$:$Yb^{3+}$,$Er^{3+}$ UCNPs, silica shell, gold nanoparticles, and gold shell were synthesized using modified procedures as previously reported.[17–19]

In a typical synthesis of $NaYF_4$:$Yb^{3+}$,$Er^{3+}$ UCNPs, 1.0 mmol rare-earth acetates (Y/Yb/Er = 78 : 20 : 2) with 6 mL of oleic acid and 15 mL of 1-octadecene were added to a flask under vigorous stirring. The solution was heated to 100 °C under vacuum conditions to remove oxygen and residual water. After cooling to 50 °C, a methanol solution (10 mL) containing 4.0 mmol of $NH_4F$ and 2.5 mmol of NaOH was added. The resulting solution was kept at 50 °C for 30 min. After methanol was evaporated, the solution was heated to 300 °C under an argon atmosphere for 90 min. The nanoparticles were precipitated by addition of ethanol and isolated *via* centrifugation.

For the formation of 10 nm silica shell, 0.5 mmol of $NaYF_4$:$Yb^{3+}$,$Er^{3+}$ UCNPs in 20 mL of cyclohexane were mixed with 1 mL of CO-520 and stirred for 10 min. Then, 4 mL of CO-520 and 0.8 mL of concentrated ammonia were added and sonicated for 20 min. After that, 0.2 mL of tetraethyl orthosilicate (TEOS) was slowly added, and the mixture was stirred for 48 h at room temperature. The nanoparticles were precipitated with acetone and washed 3 times with 1 : 1 volume of ethanol/water solution. The silica thicknesses were adjusted by varying the contents of TEOS (0.02 mL of TEOS for 2 nm $SiO_2$ shell and 0.4 mL of TEOS for 18 nm $SiO_2$ shell).

For the amine functionalization of $NaYF_4$:$Yb^{3+}$,$Er^{3+}$@$SiO_2$ surface, 0.5 mmol of $NaYF_4$:$Yb^{3+}$,$Er^{3+}$@$SiO_2$ nanoparticles were dispersed in 20 mL of ethanol by sonication. Then, 1.3 mL of concentrated ammonia was added and stirred for 10 min under a sealed condition. After that, 1.0 mL of 3-aminopropyltriethoxysilane was slowly added and stirred for 24 h under a sealed condition. In order to improve the modification effect, the solution was then stirred at 70 °C for 2 h in water bath. The nanoparticles were centrifuged at 8000 rpm and washed 2 times with ethanol. The final products were dispersed in 40 mL of deionized (DI) water.

For the formation of gold seeds, 0.1 g of NaOH with 12 μL of 80% tetrakis (hydroxymethyl) phosphonium chloride were added to 45 mL of DI water under vigorous stirring. Then, 2 mL of 1% chloroauric acid ($HAuCl_4$) was quickly added. The solution was stirred for 3 h in darkroom, and then centrifuged at 12 000 rpm. Gold seeds were washed 2 times with ethanol before dispersed in 10 mL of DI water. The formation procedure of gold nanoparticles was the same as that of gold seeds, except that the content of $HAuCl_4$ was 4 mL. After the synthesis of gold seeds (or gold nanoparticles), 10 mL of amine-modified $NaYF_4$:$Yb^{3+}$,$Er^{3+}$@$SiO_2$ aqueous solution was slowly dropped into 5 mL of gold seeds (or gold nanoparticles) solution. With 6 h of curing, gold seeds (or gold nanoparticles) were attached onto the surface of $NaYF_4$:$Yb^{3+}$,$Er^{3+}$@$SiO_2$ nanoparticles. The solution was centrifuged at 5500 rpm and washed 2 times with ethanol. The as-prepared $NaYF_4$:$Yb^{3+}$,$Er^{3+}$@$SiO_2$@Au nanoparticles were then dispersed in 10 mL of DI water.

For gold shell growth, 0.025 g of potassium carbonate was dissolved in 100 mL of DI water. After 10 min, 1.5 mL of 1% $HAuCl_4$ was added. The solution was aged for 24 h in darkroom. Then, 10 mL of above solution was mixed with 5 mL of gold seeds attached $NaYF_4$:$Yb^{3+}$,$Er^{3+}$@$SiO_2$ nanoparticles, and stirred for 10 min. A reducing agent formaldehyde (35%, 36 μL) was then introduced dropwise. Under vigorous stirring, a black precipitate was observed few minutes later. The solution was centrifuged at 5500 rpm and washed 2 times with ethanol. The $NaYF_4$:$Yb^{3+}$,$Er^{3+}$@$SiO_2$@Au core–shell nanostructures were dispersed in 10 mL DI water for further study.

### Characterization

The nanoparticle morphology was recorded on a Tecnai G2 transmission electron microscopy (TEM). A temperature-controlled heating system was used for temperature-dependent UCL spectra measurement. Room-temperature and temperature-dependent UCL spectra were measured by a portable spectrometer (Maya 2000, Ocean Optics Co.) using a continuous 975 nm diode laser as the excitation source. An excitation power of about 120 mW was used, corresponding to a power density of 3 W $cm^{-2}$. For the measurement of temperature-dependent UCL spectra of solution samples, a heating platform was used for heating the solution and the temperature was monitored by a thermocouple immersed into the solution. Absorption spectra of solution samples were measured by a Cary 5000 UV-Vis-NIR spectrophotometer. For measurement of the photothermal conversion properties of UCNPs in solution, the 975 nm laser was used as the radiation source, and the temperature was monitored by a thermocouple immersed into the solution.

## Results and discussion

### Structure and morphology

Fig. 1(a–d) shows typical TEM images of $NaYF_4$:$Yb^{3+}$,$Er^{3+}$ UCNPs before and after $SiO_2$ shell growth. It can be seen that the uncoated $NaYF_4$:$Yb^{3+}$,$Er^{3+}$ UCNPs are monodispersed and can self-assemble onto the surface of copper film (Fig. 1a). After $SiO_2$ shell growth, the nanoparticles could be re-dispersed in aqueous solution with a high monodispersity, which is favorable for their further biomedical applications. The average diameter of the $NaYF_4$:$Yb^{3+}$,$Er^{3+}$@$SiO_2$ nanoparticles increased by 4, 20, and 36 nm compared to the uncoated $NaYF_4$:$Yb^{3+}$,$Er^{3+}$ core (Fig. 1b–d), indicating the successful coating of 2, 10, and 18 nm $SiO_2$ shells around the $NaYF_4$:$Yb^{3+}$,$Er^{3+}$ core. Fig. 1(e) shows a clear $NaYF_4$:$Yb^{3+}$,$Er^{3+}$@$SiO_2$ core–shell nanostructures. The corresponding energy-dispersive X-ray analysis (EDX) proves the existence of Si and O elements (Fig. 1(f)), indicating the formation of $SiO_2$ shell around $NaYF_4$:$Yb^{3+}$,$Er^{3+}$ core.

 

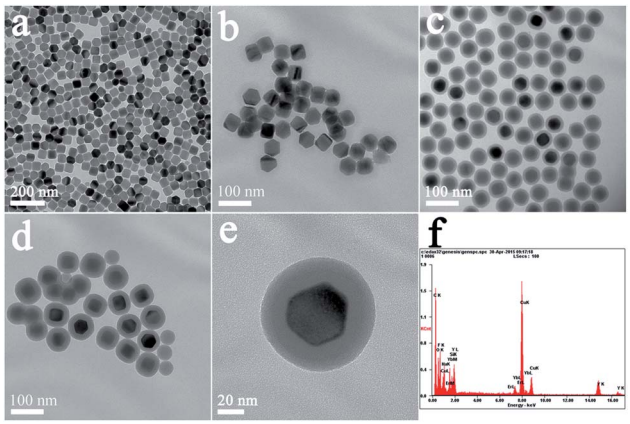


Fig. 1 TEM images of (a) $NaYF_4$:$Yb^{3+}$,$Er^{3+}$ UCNPs, and $NaYF_4$:-$Yb^{3+}$,$Er^{3+}$@$SiO_2$ core–shell nanostructures with different $SiO_2$ shell thicknesses: (b) 2 nm, (c) 10 nm, (d) 18 nm. (e) The magnified TEM image of single $NaYF_4$:$Yb^{3+}$,$Er^{3+}$@$SiO_2$ core–shell nanostructures. (f) The corresponding EDX spectrum of (e).

After amine modification, gold nanoparticles with average diameter of ~9.3 nm were attached onto the surface of $NaYF_4$:$Yb^{3+}$,$Er^{3+}$@$SiO_2$ nanoparticles. As shown in Fig. 2(a–c), $NaYF_4$:$Yb^{3+}$,$Er^{3+}$@$SiO_2$@Au nanostructures with different $SiO_2$ spacer layer thicknesses were constructed after the gold nanoparticles adsorption. Taking advantage of $NaYF_4$:-$Yb^{3+}$,$Er^{3+}$@$SiO_2$ nanoparticles attached with gold seeds as the precursors, gold shells were then successfully obtained by introducing additional $HAuCl_4$ and reductant into the solution. It can be seen from Fig. 2(d–f) that continuous gold shells with the average thickness of 15 nm have grown on the surface of $NaYF_4$:$Yb^{3+}$,$Er^{3+}$@$SiO_2$ nanoparticles. The coated gold shell reduced the monodispersity of $NaYF_4$:$Yb^{3+}$,$Er^{3+}$@$SiO_2$@Au nanostructures in aqueous solution, and even presented a black precipitate in final products, indicating the strong absorption of visible light.

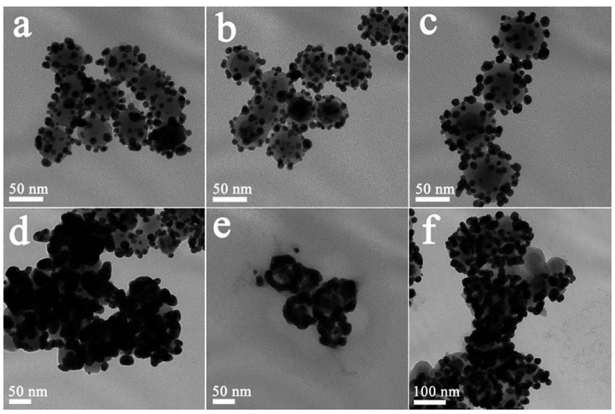


Fig. 2 TEM images of gold particles adsorbed $NaYF_4$:-$Yb^{3+}$,$Er^{3+}$@$SiO_2$@Au nanostructures with different $SiO_2$ shell thicknesses: (a) 2 nm, (b) 10 nm, (c) 18 nm, and gold shell coated $NaYF_4$:$Yb^{3+}$,$Er^{3+}$@$SiO_2$@Au nanostructures with different $SiO_2$ shell thicknesses: (d) 2 nm, (e) 10 nm, (f) 18 nm.

## Upconversion luminescence properties

The upconversion emission spectra of $NaYF_4$:$Yb^{3+}$,$Er^{3+}$@$SiO_2$@-Au nanostructures were collected in aqueous solution under 975 nm laser excitation. It can be seen from Fig. 3(a–c) that green and red upconversion emissions centered at around 525, 545, and 660 nm are observed for all samples, corresponding to the $^2H_{11/2} \rightarrow {}^4I_{15/2}$, $^4S_{3/2} \rightarrow {}^4I_{15/2}$, and $^4F_{9/2} \rightarrow {}^4I_{15/2}$ transitions of $Er^{3+}$ ions, respectively. With gold nanoparticles attachment, an obvious reduction in UCL intensity can be found when 2 nm thickness of $SiO_2$ was used as the spacer layer (Fig. 3a). The UCL intensity will further attenuate with the formation of gold shell, *e.g.*, the integral UCL intensities decreased over 85% and 98% after the gold nanoparticles adsorption and gold shell coating, respectively (Fig. 3d). It is well known that there exits an interaction between noble metals and UCNPs, depending on the distance of UCNPs from the metal surface.[20] Therefore, we attempt to further regulate the dominant effect of the gold nanostructures on UCL properties by increasing the $SiO_2$ spacer layer thicknesses. Fig. 3(b) and (c) show the UCL intensities of $NaYF_4$:$Yb^{3+}$,$Er^{3+}$@$SiO_2$@Au nanostructures with increasing the $SiO_2$ spacer layer thicknesses to 10 and 18 nm, respectively. It can be found that significant UCL quenching effect still exists as the presence of gold nanoparticles and gold shell (Fig. 3d). It means that the existence of gold nanostructures (including gold particles and gold shell) led to an obvious quenching in UCL intensities, and the spacer layer thickness was not the dominant factor that governed the UCL intensities of $NaYF_4$:$Yb^{3+}$,$Er^{3+}$@$SiO_2$@Au nanostructures.

Three interactions between metal nanostructures and UCNPs can influence the UCL intensities of UCNPs: (a) an increase of the excitation rate by local field enhancement (LFE); (b) an increase of the emission rate by surface-plasmon-coupled emission (SPCE); (c) energy transfer from UCNPs to metal nanostructures (ET).[21] LFE and SPCE factors account for the

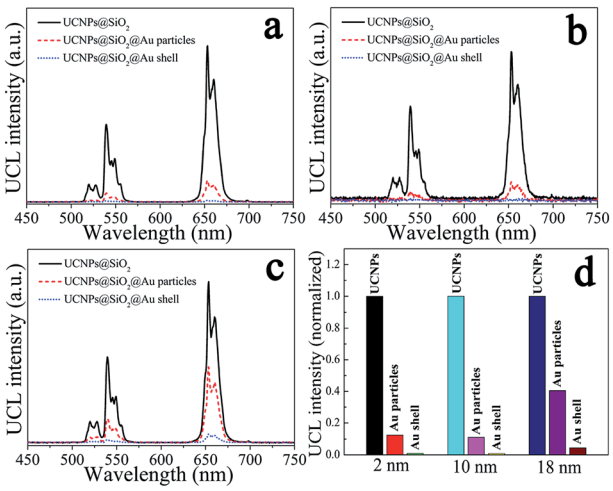


Fig. 3 Room-temperature UCL spectra of $NaYF_4$:$Yb^{3+}$,$Er^{3+}$@$SiO_2$, $NaYF_4$:$Yb^{3+}$,$Er^{3+}$@$SiO_2$@Au nanoparticles and $NaYF_4$:-$Yb^{3+}$,$Er^{3+}$@$SiO_2$@Au shell with different $SiO_2$ shell thicknesses: (a) 2 nm, (b) 10 nm, (c) 18 nm, and (d) the corresponding UCL intensities comparison.

metal-induced UCL enhancement.[22] However, the energy transfer from UCNPs to metal nanostructures would result in an obvious quenching in UCL intensities.[23] In order to understand the interaction between gold nanostructures and UCNPs, we further characterized the UV-Vis-NIR absorption spectra of gold nanoparticles and gold shell. As shown in Fig. 4(a), a surface plasmon resonance (SPR) peak centered at around 550 nm can be observed for gold nanoparticles, which overlays well with the upconversion emission peaks at around 525 and 545 nm, and partially overlays with the emission peak at around 660 nm. Given that UCL was suppressed rather than enhanced by gold nanoparticles, it is reasonable to believe that ET instead of SPCE plays the dominant role in regulating the UCL intensities of $NaYF_4$:$Yb^{3+}$,$Er^{3+}$ UCNPs. Compared with the sharp absorption peak of gold nanoparticles, a wide absorption band from visible to NIR region can be observed for gold shell (Fig. 4b). Due to the strong absorption of all upconversion emissions as well as the 975 nm excitation light, the UCL was quenched after the gold shell growth. The obvious enhancement in photothermal conversion properties in the presence of gold nanostructures (will be discussed later) also proved the huge energy extraction from upconversion emission, and consequently led to a significant reduction in UCL intensities. Previous study on enhancing the UCL by gold shell tuned the SPR peak to the NIR region (900 nm) by reducing the shell thickness to 3 nm.[24] We thus believe that a thin gold shell is necessary for the enhancement of UCL.

### Temperature sensing and photothermal properties

Due to the narrow energy gap between $^2H_{11/2}$ and $^4S_{3/2}$ energy levels of $Er^{3+}$ ions, a thermal equilibrium exists between them.[25] Therefore, the intensity ratio ($R_{HS}$) of $^2H_{11/2} \rightarrow {}^4I_{15/2}$ and $^4S_{3/2} \rightarrow {}^4I_{15/2}$ transitions of $Er^{3+}$ ions is sensitive to temperature. According to Boltzmann's distribution, the intensity ratio $R_{HS}$ as a function of temperature can be expressed as:[26]

$$R_{HS} = R_{HS}(0)\exp(-\Delta E/kT) \quad (1)$$

where $\Delta E$ is the energy gap between $^2H_{11/2}$ and $^4S_{3/2}$ energy levels, $k$ is the Boltzmann constant, $T$ is the absolute temperature and $R_{HS}(0)$ is a constant. This relation provides a simple non-contact method for real-time temperature measurements.

Fig. 5(a) shows the dependence of $\ln(R_{HS})$ on the inverse temperature for $NaYF_4$:$Yb^{3+}$,$Er^{3+}$ UCNPs with and without gold nanoparticles and gold shell. In accordance with eqn (1), all the samples show a good linear relation of $\ln(R_{HS})$ *versus* $1/T$. It means that the temperature can be accurately measured from the intensity ratio of 525 and 545 nm emissions. In addition, almost the same relations of $R_{HS}$ *vs.* $1/T$ are obtained for three samples, indicating that the existence of gold nanostructures has little effects on the temperature sensing properties of $NaYF_4$:$Yb^{3+}$,$Er^{3+}$ UCNPs. Therefore, $NaYF_4$:$Yb^{3+}$,$Er^{3+}$@$SiO_2$@Au nanostructures can be used as the temperature sensing probes for real-time temperature monitoring, without altering the temperature sensing properties of UCNPs.

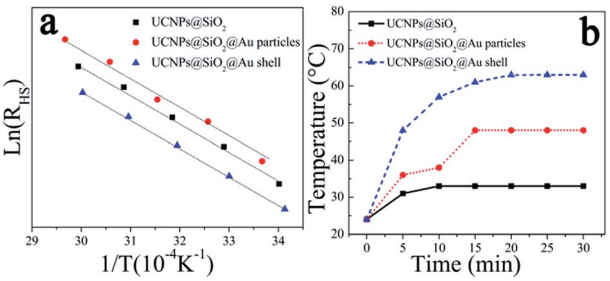


Fig. 5 (a) Plots of $\ln(R_{HS})$ *vs.* $1/T$ and (b) photothermal conversion properties of $NaYF_4$:$Yb^{3+}$,$Er^{3+}$@$SiO_2$, $NaYF_4$:$Yb^{3+}$,$Er^{3+}$@$SiO_2$@Au nanoparticles and $NaYF_4$:$Yb^{3+}$,$Er^{3+}$@$SiO_2$@Au shell.

To assess the photothermal conversion properties for possible biomedical applications, the change of the temperature of $NaYF_4$:$Yb^{3+}$,$Er^{3+}$@$SiO_2$@Au nanostructures in aqueous solution were measured under the exposure to 975 nm laser with the pump power of 1.73 W. As depicted in Fig. 5(b), the temperature of $NaYF_4$:$Yb^{3+}$,$Er^{3+}$ UCNPs increased ~9 °C within 10 min. This temperature rises can be attributed to the low quantum yields of UCNPs, which lead to most of the energy consumed in the form of heat. Therefore, the temperature of $NaYF_4$:$Yb^{3+}$,$Er^{3+}$ UCNPs can rise rapidly using 975 nm NIR light as the radiation source. As the presence of gold nanostructures, the photothermal conversion properties of $NaYF_4$:$Yb^{3+}$,$Er^{3+}$ UCNPs are dramatically improved. For instance, the temperature increased by ~24 and ~39 °C with gold nanoparticles attachment and gold shell coating, respectively. This photothermal conversion results outperform the previous records reported in literature,[16] suggesting great promise for further clinical applications. The improved photothermal conversion properties can be attributed to the precise position and high intensity of the SPR peak (Fig. 4) regulated by the appropriate dimension of metal nanostructures, including the size of metal nanoparticles and the thickness of metal shells. The gold nanostructures can absorb energy from UCNPs, and then converts it into heat.

The above results suggest that $NaYF_4$:$Yb^{3+}$,$Er^{3+}$@$SiO_2$@Au nanostructures would be ideal diagnostic and therapeutic tool to be used *in vitro* and *in vivo*, due to their ability of integrating UCL, temperature sensing, and photothermal therapy simultaneously. Considering the big particle size and the low dispersion in aqueous solution of gold shell coated $NaYF_4$:$Yb^{3+}$,$Er^{3+}$@$SiO_2$@Au nanostructures, we believe that gold nanoparticles coated $NaYF_4$:$Yb^{3+}$,$Er^{3+}$@$SiO_2$@Au nanostructures with excellent

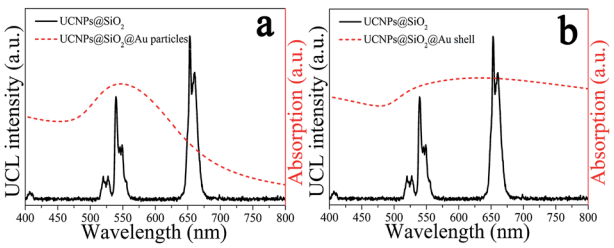


Fig. 4 (a) UCL spectra of $NaYF_4$:$Yb^{3+}$,$Er^{3+}$@$SiO_2$ nanostructures (black line) and absorption spectra of gold nanoparticles (red line), (b) UCL spectra of $NaYF_4$:$Yb^{3+}$,$Er^{3+}$@$SiO_2$ nanostructures (black line) and absorption spectra of gold shell (red line).

photothermal conversion properties and high dispersion in aqueous solution are preferable as multifunctional nanomaterials in biomedical fields.

## Conclusions

In summary, $NaYF_4$:$Yb^{3+}$,$Er^{3+}$@$SiO_2$@Au heterogeneous nanostructures have been successfully synthesized, and their multifunctional properties including UCL, temperature sensing and photothermal conversion were systemically studied. The results show that the $NaYF_4$:$Yb^{3+}$,$Er^{3+}$@$SiO_2$@Au nanostructures are capable of simultaneously providing UCL, photothermal therapy, and real-time temperature monitoring. The presence of gold nanostructures has dramatically improved the photothermal conversion properties of $NaYF_4$:$Yb^{3+}$,$Er^{3+}$ UCNPs without altering their temperature sensing properties. The temperature increased by ~39 °C with gold shell coating, representing the best photothermal conversion result among UCNPs. In addition, the UCL intensities of $NaYF_4$:$Yb^{3+}$,$Er^{3+}$ UCNPs exhibit an obvious attenuation with gold nanoparticles attachment and gold shell coating, and it was found that they were independent of the $SiO_2$ spacer layer thicknesses, due to the efficient energy transfer from UCNPs to the gold nanostructures.

## Acknowledgements

The authors acknowledge financial support from the National Key Basic Research Program of China (973 Program, 2014CB648300), the National Natural Science Foundation of China (21422402, 21674050, 61136003), the Natural Science Foundation of Jiangsu Province (BK20160073, BK20140060, BK20130037, BM2012010), Program for Jiangsu Specially-Appointed Professors (RK030STP15001), Program for New Century Excellent Talents in University (NCET-13-0872), Specialized Research Fund for the Doctoral Program of Higher Education (20133223110008), the Synergetic Innovation Center for Organic Electronics and Information Displays, the Priority Academic Program Development of Jiangsu Higher Education Institutions (PAPD), the NUPT "1311 Project", the Six Talent Plan (2012XCL035), the 333 Project (BRA2015374) and the Qing Lan Project of Jiangsu Province. This work was also sponsored by NUPTSF (NY216025).

## Notes and references

1 M. K. Tsang, G. X. Bai and J. H. Hao, *Chem. Soc. Rev.*, 2015, **44**, 1585–1607.
2 C. X. Li and J. Lin, *J. Mater. Chem.*, 2010, **20**, 6831–6847.
3 Y. Sun, X. J. Zhu, J. J. Peng and F. Y. Li, *ACS Nano*, 2013, **7**, 11290–11300.
4 L. Cheng, K. Yang, Y. G. Li, X. Zeng, M. W. Shao, S. T. Lee and Z. Liu, *Biomaterials*, 2012, **33**, 2215–2222.
5 L. Cheng, K. Yang, Y. G. Li, J. H. Chen, C. Wang, M. W. Shao, S. T. Lee and Z. Liu, *Angew. Chem., Int. Ed.*, 2011, **123**, 7523–7528.
6 S. S. Han, X. Qin, Z. F. An, Y. H. Zhu, L. L. Liang, Y. Han, W. Huang and X. G. Liu, *Nat. Commun.*, 2015, **7**, 13059.
7 X. G. Liu, C. H. Yan and J. A. Capobianco, *Chem. Soc. Rev.*, 2015, **44**, 1299.
8 W. Wei, T. C. He, X. Teng, S. X. Wu, L. Ma, H. Zhang, J. Ma, Y. H. Yang, H. Y. Chen, Y. Han, H. D Sun and L. Huang, *Small*, 2012, **8**, 2271–2276.
9 H. Y. Xing, W. B. Bu, S. J. Zhang, X. P. Zheng, M. Li, F. Chen, Q. J. He, L. P. Zhou, W. J. Peng, Y. Q. Hua and J. L. Shi, *Biomaterials*, 2012, **33**, 1079–1089.
10 F. Vetrone, R. Naccache, A. Zamarrón, A. J. de la Fuente, F. S. Rodríguez, L. M. Maestro, E. M. Rodriguez, D. Jaque, J. G. Solé and J. A. Capobianco, *ACS Nano*, 2010, **4**, 3254–3258.
11 D. M. Yang, P. A. Ma, Z. Y. Hou, Z. Y. Cheng, C. X. Li and J. Lin, *Chem. Soc. Rev.*, 2015, **44**, 1416–1448.
12 C. R. Lecuna, R. M. Rodríguez and R. Valiente, *Chem. Mater.*, 2011, **23**, 3442–3448.
13 J. C. Boyer and F. C. J. M. van Veggel, *Nanoscale*, 2010, **2**, 1417–1419.
14 Q. Y. Shao, L. L. Ouyang, L. F. Jin and J. Q. Jiang, *Opt. Express*, 2015, **23**, 30057–30066.
15 B. Dong, S. Xu, J. Sun, S. Bi, D. Li, X. Bai, Y. Wang, L. P. Wang and H. W. Song, *J. Mater. Chem.*, 2011, **21**, 6193–6200.
16 Y. Song, G. X. Liu, X. T. Dong, J. X. Wang, W. S. Yu and J. M. Li, *RSC Adv.*, 2014, **4**, 62802–62808.
17 H. S. Qian and Y. Zhang, *Langmuir*, 2008, **24**, 12123–12125.
18 L. Li, K. Green, H. Hallen and S. F. Lim, *Nanotechnology*, 2015, **26**, 025101.
19 H. Zhang, Y. J. Li, I. A. Ivanov, Y. Q. Qu, Y. Huang and X. F. Duan, *Angew. Chem., Int. Ed.*, 2010, **49**, 2865–2868.
20 M. Saboktakin, X. C. Ye, S. J. Oh, S. H. Hong, A. T. Fafarman, U. K. Chettiar, N. Engheta, C. B. Murray and C. R. Kagan, *ACS Nano*, 2012, **6**, 8758–8766.
21 P. Y. Yuan, Y. H. Lee, M. K. Gnanasammandhan, Z. P. Guan, Y. Zhang and Q. H. Xu, *Nanoscale*, 2012, **4**, 5132–5137.
22 W. Deng, L. Sudheendra, J. B. Zhao, J. X. Fu, D. Y. Jin, I. M. Kennedy and E. M. Goldys, *Nanotechnology*, 2011, **22**, 325604.
23 Z. Q. Li, L. M. Wang, Z. Y. Wang, X. H. Liu and Y. J. Xiong, *J. Phys. Chem. C*, 2011, **115**, 3291–3296.
24 A. Priyam, N. M. Idris and Y. Zhang, *J. Mater. Chem.*, 2012, **22**, 960–965.
25 J. N. Shan, W. J. Kong, R. Wei, N. Yao and Y. G. Ju, *J. Appl. Phys.*, 2010, **107**, 054901.
26 M. D. Shinn, W. A. Sibley, M. G. Drexhage and R. N. Brown, *Phys. Rev. B: Condens. Matter Mater. Phys.*, 1983, **27**, 6635–6648.